INVITED PAPER *Special Issue on the IEEE International Conference on SISPAD '02*

An Adaptive Grid Approach for the Simulation of Electromigration Induced Void Migration*

Hajdin CERIC[†a)] ***and*** **Siegfried SELBERHERR**[†], ***Nonmembers***

SUMMARY For tracking electromigration induced evolution of voids a diffuse interface model is applied. We assume an interconnect as two-dimensional electrically conducting via which contains initially a circular void. The diffuse interface governing equation was solved applying a finite element scheme with a robust local grid adaptation algorithm. Simulations were carried out for voids exposed to high current. An influence of the void dynamics on the resistance of interconnect is investigated. In the case of the interconnect via it was shown that a migrating void exactly follows the current flow, retaining its stability, but due to change of shape and position causes significant fluctuations in interconnect resistance.

key words: *electromigration, diffuse interface model, grid adaptation, void evolution, finite element method*

1. Introduction

Failure of metallic interconnects in integrated circuits caused by electromigration has long been a key reliability concern which is further accentuated by the continuing trend of miniaturization. The phenomenon of electromigration is a mechanism for transport of matter by high electric current densities which produce damage in the interconnect lines. Failure results either from voids growing over the entire line width or extrusions which cause short circuits to neighboring lines.

Modeling the micromechanics of void evolution is a long-standing scientific problem. It began with sharp interface models requiring an explicit finite element tracking of void surfaces during the course of evolution [8]. Later, prompted by the complexity of void surfaces, diffuse interface models were introduced [1]. Diffuse interface models circumvent computationally costly explicit surface tracking by application of a smooth order parameter field for representation of void structures. An alternative diffuse interface model based on the double obstacle potential was proposed in [4] where the computation is simplified by reduction of order parameter profiles evaluation only to the void-metal interfacial area.

The main disadvantages of these diffuse interface models [3], [4] is their requirement of structured underlaying grids for the order parameter evaluation and also their restricted facility to reach higher resolution of an order parameter profile in the void-metal interfacial area. To overcome these drawbacks we solve the diffuse interface model governing equation with a finite element scheme coupled with a powerful grid adaptation algorithm. The robustness of the developed finite element approach with respect to the underlying grid structure makes it possible to efficiently simulate the damage induced by electromigration in complex interconnect geometries.

2. Theoretical Formulation

We assumed unpassivated monocrystal isotropic interconnects where stress phenomena can be neglected. An interconnect is idealized as two-dimensional electrically conducting via which contains initially a circular void. For simplicity we also neglect the effects of grain boundaries and lattice diffusion. In this case there are two main forces which influence the shape of the evolving void interface: the chemical potential gradient and electron wind. The first force causes self-diffusion of metal atoms on the void interface and tends to minimize energy which results in circular void shapes. The electron wind force produces asymmetry in the void shape depending on the electrical field gradients.

Including contributions from both electromigration and chemical potential-driven surface diffusion gives the total surface atomic flux, $\mathbf{J_A} = J_A\mathbf{t}$, where $\mathbf{t}$ is the unit vector tangent to the void surface [8], [9]

$$J_A = D_s(-|e|Z^* E_s + \gamma_s \Omega\, \mathbf{t} \cdot \nabla_{\mathbf{s}} \kappa) \tag{1}$$

Z^* is the effective valence, e is the charge of an electron, $E_s \equiv \mathbf{E_s} \cdot \mathbf{t}$ is the local component of the electric field tangential to the void surface, κ is the local surface curvature, and ∇_s is the surface gradient operator; $\kappa \equiv \nabla \cdot \mathbf{n}$, where $\mathbf{n}$ is the local unit vector normal to the void surface. Further, γ_s is the surface energy, Ω is the volume of an atom, and D_s is given trough Arrhenius' law:

$$D_s = \frac{D_0 \delta_s}{k_B T} \exp\Big(\frac{-Q_s}{k_B T}\Big) \tag{2}$$

Here, δ_s is the thickness of the diffusion layer, k_B is Boltzmann's constant, T is the temperature, Q_s is the activation energy for the surface diffusion, and D_0 is the pre-exponential for mass diffusion. Equation (1) is the Nernst-Einstein equation, where the sum in the

Manuscript received September 21, 2002.

[†]The authors are with Institute for Microelectronics, TU Vienna, Austria.

a) E-mail: Ceric@iue.tuwien.ac.at

*This paper was presented at SISPAD 2002.

parentheses on the right side expresses the driving force. Mass conservation gives the void propagation velocity normal to the void surface, v_n, through the continuity equations [9]–[11],

$$v_n = -\Omega \cdot \nabla_s \mathbf{J_A}. \tag{3}$$

The electric field $\mathbf{E}$ in the interconnect is irrotational, $\nabla \times \mathbf{E} = \mathbf{0}$ and it can be written as the gradient of the electric potential, i.e.,

$$\mathbf{E} \equiv -\nabla \mathbf{V}. \tag{4}$$

The field is also solenoidal, i.e.,

$$\nabla \cdot \mathbf{E} = \mathbf{0}. \tag{5}$$

Equations (4) and (5) imply that the potential V obeys Laplace's equation,

$$\Delta V = 0 \tag{6}$$

The void surface and the interconnect's edges are modeled as insulating boundaries, i.e., $\nabla V \cdot \mathbf{n} = 0$ at these boundaries.

3. Applied Diffuse Interface Model

Direct numerical implementation of Eqs. (1)–(6) demands explicit tracking of the moving void-metal interface. The interface is described by specifying a large number of points on it. Over the time the void-metal interface evolves and changes morphology and even more points may be required to accurately describe it. Such techniques are very complicated to implement and also tend to have rather poor numerical stability.

In the diffuse interface models void and metal area are presented through the order parameter ϕ which takes values $+1$ in the metal area, -1 in the void area and $-1 < \phi < +1$ in the void-metal interface area. Demanding explicit tracking of the void-metal interface is not needed and models do not require boundary conditions to be enforced at the moving boundary. Diffuse interface models are, as we will see in the next sections, quite simple to implement numerically.

The model equations for the void evolving in an unpassivated interconnect line are the balance equation for the order parameter ϕ [1]–[4],

$$\frac{\partial \phi}{\partial t} = \frac{2D_s}{\epsilon\pi} \nabla \cdot (\nabla \mu - |e| Z^* \nabla V) \tag{7}$$

$$\mu = \frac{4\Omega\gamma_s}{\epsilon\pi}(f'(\phi) - \epsilon^2 \Delta\phi) \tag{8}$$

and for the electrical field

$$\nabla \cdot (\sigma(\phi) \nabla V) = 0 \tag{9}$$

where μ is the chemical potential, $f(\phi)$ is the double obstacle potential as defined in [5], [6], and ϵ is a parameter controlling the void-metal interface width. The electrical conductivity was taken to vary linearly from the metal ($\sigma = \sigma_{metal}$) to the void area ($\sigma = 0$) by setting $\sigma = \sigma_{metal}(1 + \phi)/2$. Equations (7) and (9) are solved on the two-dimensional polygonal interconnect area T.

It has been proven [2], [4] that in the asymptotic limit for $\epsilon \to 0$ the diffuse interface model defined by Eqs. (7)–(9) describes the same voids-metal interface behavior like Eqs. (1)–(6). The width of the void-metal diffuse interface is approximately $\epsilon\pi/2$, and in order to numerically handle sufficiently thin interfaces one needs a very fine locally placed grid around it.

4. Numerical Implementation

Equations (7)–(9) are solved by means of the finite element method on the sequence of the grids $\Lambda_h(t_0 = 0), \Lambda_h(t_1), \Lambda_h(t_2)$ each one adapted to the position of the void-metal interface from the previous time step. The initial grid $\Lambda_h(0)$ is produced by refinement of some basic triangulation T_h of area T according to the initial profile of order parameter ϕ. The motivation of grid adaptation is to construct and maintain a fine triangulated belt of width $\epsilon\pi$ in the interconnect area where $-1 < \phi < +1$, respectively, where the void-metal interface area is placed.

4.1 Setting of the Initial Order Parameter Profile and Initial Grid Refinement $\Lambda_h(0)$

The initial order parameter profile depends on the initial shape of the void $\Gamma(0)$ and can be expressed as

$$\phi(x,y) = \begin{cases} +1 & \text{if} \quad d > \frac{\epsilon\pi}{2}, \\ \sin\left(\frac{d}{\epsilon}\right) & \text{if} \quad |d| \le \frac{\epsilon\pi}{2}, \\ -1 & \text{if} \quad d < -\frac{\epsilon\pi}{2} \end{cases} \tag{10}$$

Where $d = dist(P(x,y), \Gamma(0))$ is the signed normal distance of the point from the initial interface $\Gamma(0)$. To obtain sufficient resolution of this initial profile, the basic grid T_h is transformed into grid $\Lambda_h(0)$ obeying the following *initial grid refinement criterion (IGRC)* for the circular void with center O and radius r:

$$|dist(C_K, O) - r| \le \frac{\epsilon\pi}{2} \quad \wedge \quad h_K > \frac{\epsilon\pi}{n} \tag{11}$$

n is the chosen number of grid elements across the void-metal interface width, h_K is the longest vertex of the triangle K, and C_K is its center of gravity. Now an adaptive algorithm defined in Sect. 4.4 transforms the basic grid T_h into initial grid $\Lambda_h(0)$ according to $IGRC$.

4.2 Finite Element Scheme

Let $\Lambda_h(t_n)$ be a triangulation of the area T at the discrete time t_n, and let $\{\phi_i^{n-1}\}_{i=0}^{N-1}$ be discrete nodal values of the order parameter on this triangulation.

A finite element based iteration for solving (7) on grid $\Lambda_h(t_n)$ and evaluating the order parameter at the time $t_{n+1} = t_n + \Delta t$ consists of two steps [12]:
Step 1. For the kth iteration of $n+1$th time step the linear system of equations has to be solved:

$$\epsilon\frac{\pi}{2}M_{ii}\phi_i^{n+1,k} + \Delta t D_s K_{ii}\mu_i^{n+1,k} = \alpha_i \quad (12)$$

$$M_{ii}\mu_i^{n+1,k} - \tau\left(\frac{1}{\epsilon}M_{ii} + \epsilon K_{ii}\right)\phi_i^{n+1,k} = \beta_i, \quad (13)$$

where

$$\alpha_i = \epsilon\frac{\pi}{2}M_{ii}\phi_i^n - \Delta t D_s \sum_{i\neq j} K_{ij}\mu_j^{n+1,k-1} \quad (14)$$

$$\beta_i = \tau\epsilon\sum_{i\neq j} K_{ij}\phi_j^{n+1,k-1} - |e|Z^* M_{ii}V_i^n \quad (15)$$

for each $i = 0, N-1$ of the nodal values $(\phi_i^{n+1}, \mu_i^{n+1})$ of the triangulation $\Lambda_h(t_n)$. $[M]_{ij}$ and $[K]_{ij}$ are the lumped mass and stiffness matrix, respectively and $\tau = \frac{4\Omega\gamma_s}{\pi}$.
Step 2. All nodal values $\{\phi_i^{n+1}\}_{i=0}^{N-1}$ are projected on $[-1, 1]$ by a function

$$\rho(x) = \max(-1, \min(1, x)). \quad (16)$$

For solving (9) a conventional finite element scheme is applied [13].

4.3 Maintaining the Grid During Simulation

After an order parameter was evaluated on the $\Lambda_h(t_n)$ a grid needs to be adapted according to the new void-metal interface position. Therefore it is necessary to extract all elements which are cut by the void-metal interface in grid $\Lambda_h(t_n)$. The following condition is used: Let us take a triangle $K \in \Lambda_h(t_n)$ and denote its vertices as P_0, P_1, P_2. The triangle K belongs to the interfacial elements if for the values of the order parameter ϕ at the triangle's vertices holds $\phi(P_0)\phi(P_1) < 0$ or $\phi(P_1)\phi(P_2) < 0$. We assume that an interface intersects each edge of the element only once. The set of all interfacial elements at the time t_n is denoted as $E(t_n)$. The centers of gravity of each triangle from the $E(t_n)$ build the interface point list $L(t_n)$. The distance of the arbitrary point Q from $L(t_n)$ is defined as

$$dist(Q, L(t_n)) = \min_{P\in L(t_n)} dist(Q, P). \quad (17)$$

Thus we can define the *transitional grid refinement criterion TGRC*

$$dist(C_K, L(t_n)) \leq \frac{\epsilon\pi}{2} \quad \wedge \quad h_K > \frac{\epsilon\pi}{n} \quad (18)$$

The grid adaption for the next time step evaluation of the order parameter ϕ is now completed with respect to $TGRC$ by as defined in the next section.

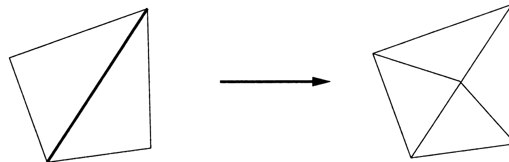

Fig. 1 Atomic refinement operation.

4.4 Grid Adaptation

The grid adaption algorithm used in this work is a version of the algorithm introduced in [7] and consists of a *grid refinement algorithm* and a *grid coarsening algorithm.* The refinement algorithm is based on recursive bisecting of triangles. A triangle is marked for refinement if it complies with some specific refinement criterion $COND$. In our application we used $COND = IGRC$ for the initial refinement and $COND = TGRC$ for the grid maintaining refinement. For every triangle of the grid, the longest one of its edges is marked as *refinement edge.* The element and its neighbor element which also contains the same refinement edge are refined by bisecting this edge (Fig. 1). We can define refinement of the element in the following way:

Algorithm 1. *refinement of the element*
```
subroutine recursive_refine(element)
{
  if neighbor has no compatible ref_edge
  recursive_refine(neighbor)
  bisect(element)
  bisect(neighbor)
}
```

Now, the overall refinement algorithm can be formulated as follows:

Algorithm 2. *refinement of the grid*
```
subroutine refine_grid(COND)
{
  for n ≤ max_refinement_depth
  {
    for all elements
    if (COND) mark element for refinement
    if no element is marked
    break refinement loop
    for all elements
    recursive_refine(element)
  }
}
```

The parameter `max_refinement_depth` limits the number of bisecting of each triangles of the grid. The grid is refined until there is no more element marked for refinement or the maximal refinement depth is reached.

The coarsening algorithm is more or less the inverse of the refinement algorithm. Each element that does not fullfil criterion $COND$ is marked for coarsening. The basic idea is to find the father element whose

refinement produced the element in consideration.

Algorithm 3. *coarsening of the element*
```
subroutine coarsen(element)
{
 get the element_father
 get the father_neighbor on ref_edge
 coarse the element_father
 coarse the father_neighbor
}
```

The following routine coarsens as many elements as possible, even more than once if allowed:

Algorithm 4. *coarsening of the grid*
```
subroutine coarsen_grid(COND)
{
 for all elements
 if (!COND) mark element for coarsening
 do
 {
  do_coarsen_once_more = false
  for all elements
  if element is marked for coarsening
  do_coarsen_once_more |= coarsen(element)
 } until do_coarsen_once_more is false
}
```

The complete adaption of the grid is reached by sequential invoking of the grid refinement and of the grid coarsening algorithm.

4.5 Solving Procedure

Combining all the components described in Sects. 4.1–4.4 we obtain the complete void evolution solving procedure (Fig. 2).

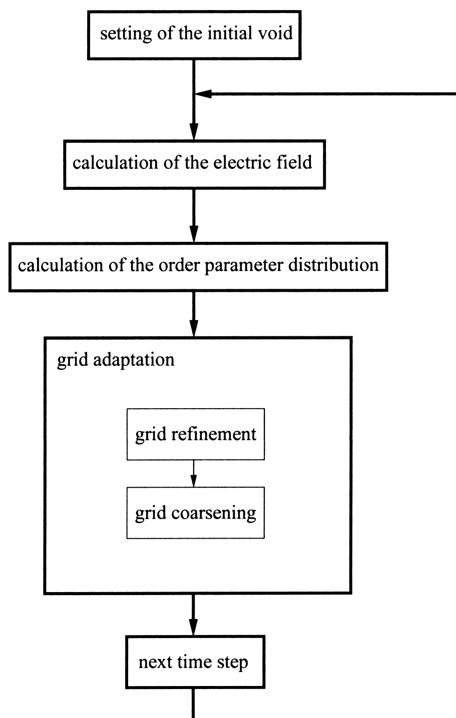

Fig. 2 Void evolution solving procedure.

5. Results

In all simulations a circle was chosen as initial void shape. The resolution of the parameter ϕ profile can be manipulated by setting parameter n which is the mean number of triangles across the void-metal interface. On Fig. 3 initial grids for $n = 1$ and $n = 5$ are presented. We consider a two-dimensional, stress free, electricaly conducting interconnect via. A constant voltage is applied between points A and B (Fig. 4). At B a refractory layer is assumed. Because of geometrical reasons there is current crowding in the adjacencies of the corners C and D. The analytical solution of Eq. (9) has at these points actually a singularity [13].

High electrical field gradients in the area around the corner points increase overall error of finite element scheme for Eq. (9) which is overcome by applying an additional refinement of the basic mesh T_h according to the local value of the electric field gradient (Fig. 5). A fine triangulated belt area which is attached to the void-metal interface at the initial simulations step follows the interfacial area throughout the simulations whereby the interconnect area outside the interface is coarsened to the level of the basic grid T_h (Fig. 6). In our simulations a void evolving through straight part of the interconnect geometry exhibits similar shape changes as observed in the earlier models [4], [8]. There is also no

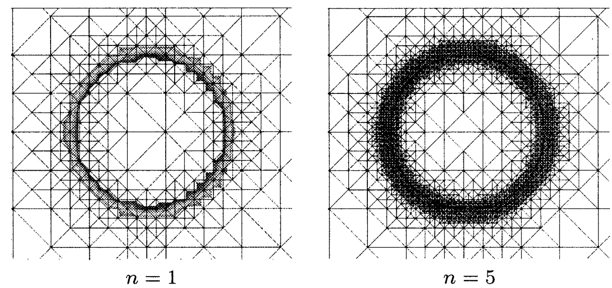

Fig. 3 Initial grid refinements.

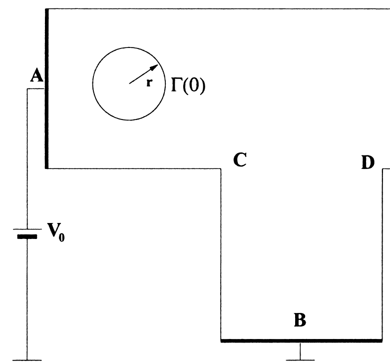

Fig. 4 Interconnect via with initial void.

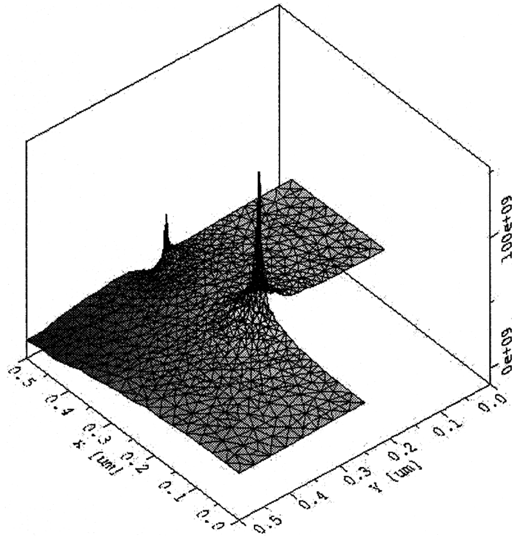

Fig. 5 Profile of the current density (in A/m^2) at the corners of the interconnect.

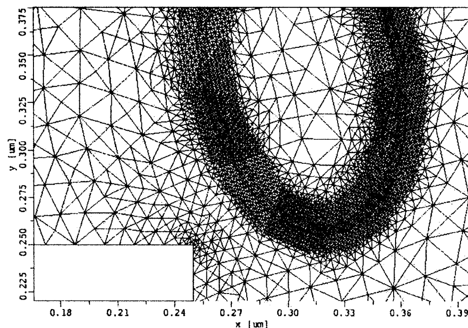

Fig. 6 Refined grid around the void in the proximity of the interconnect corner.

significant fluctuation of the resistance during this period of interconnect evolution. The situation changes when the void evolves in the proximity of the interconnect corner. Due to current crowding in this area the influence of the electromigration force on the material transport on the void surface is more pronounced than the chemical potential gradient. This unbalance leads to higher asymmetry in the void shape then observed in the straight part of the interconnect. A void evolving in the proximity of the interconnect corner causes significant fluctuations in the interconnect resistance due to void asymmetry and position. The resistance change shows a charasteristical profile with the two peaks and a valley (Fig. 7). The extremes are more pronounced for the larger initial voids.

The capability of the applied adaptation scheme is also presented in the simulation of void collision with the interconnect refractory layer (Fig. 8).

The time step Δt for the numerical scheme (12)–(15) is fitted at the simulations begin taking into account inverse proportionality of the speed of the evolving void-metal interface to the initial void radius [8]:

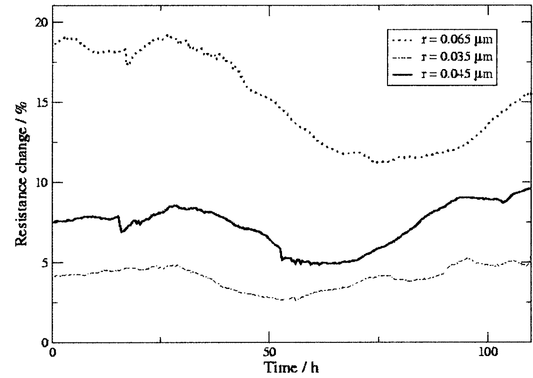

Fig. 7 Time dependent resistance change during void evolution for the different initial void radius r.

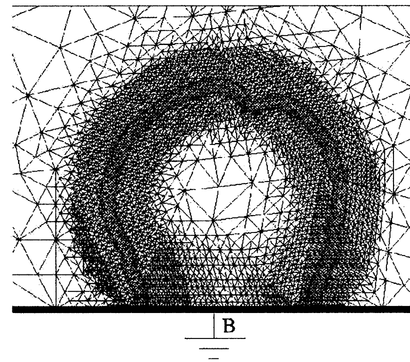

Fig. 8 Grid adaptation in the case of void collision with the refractory layer.

$$\Delta t = \frac{\epsilon \pi r l}{2 D_s |e| Z^* V_0} \tag{19}$$

l is the characteristical length of via geometry. Appropriate choice of the time step ensures that the evolving void-metal interface will stay inside the fine grid belt during the simulation. The dynamics of the evolving void-metal interface simulated with a the presented numerical scheme complies with the mass conservation law, the void area (where $\phi = -1$) remains approximately the same during the whole simulation. Notable area deviations during the simulation appear only if a relatively large factor ϵ has been chosen. As scaling length we took $l = 1\,\mu$m and for the initial void radius $r_0 = 0.035\ l$, $r_1 = 0.045\ l$, and $r_2 = 0.065\ l$. Our simulations have shown that for all considered initial void radii, voids follow the electric current direction (Fig. 9) and do not transform in slit or wedge like formations which have been found to be a main cause for a complete interconnect failure [14]. Already with $\epsilon = 0.003\ l$ good approximations are achieved. The number of elements on the cross section of the void-metal interface was chosen between 6 and 10 with the interface width of $0.0015\ l\pi$.

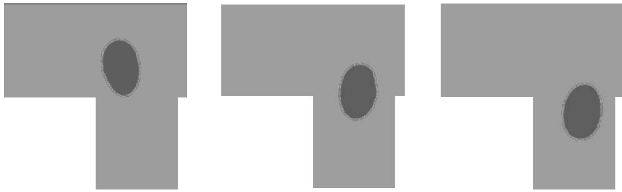

Fig. 9 Void evolving through interconnect in the electric current direction.

6. Conclusion

A governing diffuse interface equation for the order parameter coupled with the Laplace equation for the electrical field is solved using the finite element scheme. A dynamically adapted grid is maintained by a refinement-coarsening algorithm controlled by position, curvature, and width of the simulated void-metal interface which distributes the grid density in such a way that it allows an efficient simulation of evolving voids through large portions of a complex interconnect geometry. Due to high electrical current gradients in the proximity of the interconnect corners and overall asymmetry of the electrical field, voids exhibit specific faceting which was not observed in the case of straight interconnect geometries. The presented method is well suited for long time prediction of resistance change due to electromigration during the interconnect life time. The applied diffuse interface model extends readily to incorporate additional physical phenomena such as anisotropy, temperature variations, and bulk and grain boundary diffusion.

Acknowledgment

This work has been supported by the European Community *MULSIC* project IST-2000-30133.

References

[1] M. Mahadevan and R. Bradley, "Simulations and theory of electromigration-induced slit formation in unpassivated single-crystal metal lines," Phys. Rev. B, vol.59, no.16, pp.11037–11046, 1999.

[2] M. Mahadevan and R. Bradley, "Phase field model of surface electromigration in single crystal metal thin films," Physica D., vol.126, pp.201–213, 1999.

[3] M. Mahadevan, R. Bradley, and J.M. Debierre, "Simulation of an electromigration-induced edge instability in single-crystal metal lines," Europhys. Lett., vol.45, pp.680–685, Feb. 1999.

[4] D.N. Bhate, A. Kummar, and A.F. Bower, "Diffuse interface model for electromigration and stress voiding," J. Appl. Phys., vol.87, no.4, pp.1712–1721, Dec. 2000.

[5] J. Blowey and C. Elliott, "The Chan-Hilliard gradient theory for phase separation with non-smooth free energy, Part II: Numerical analysis," Euro. Jnl of Applied Mathematics, vol.3, pp.147–176, 1992.

[6] J. Blowey and C. Elliott, "The Chan-Hilliard gradient theory for phase separation with non-smooth free energy, Part I: Mathematical analysi," Euro. J. Applied Mathematics, vol.2, pp.233–279, 1991.

[7] I. Kossacky, "A recursive approach to local mesh refinement in two and three dimensions," J. Comput. Appl. Math., vol.55, pp.275–288, 1994.

[8] D.R. Fridline and A.F. Bower, "Influence of anisotropic surface diffusivity on electromigration induced void migration and evolution," J. Appl. Phys., vol.85, no.6, pp.3168–3174, 1999.

[9] Z. Suo, W. Wang, and M. Yang, "Electromigration instability: Transgranular slits in interconnects," Appl. Phys. Lett., vol.64, no.15, pp.1944–1946, 1994.

[10] Z. Suo and W. Wang, "Diffusive void bifurcation in stressed solid," J. Appl. Phys., vol.76, no.6, pp.3410–3421, 1994.

[11] P.S. Ho, "Motion of inclusion by a direct current and a temperature gradient," J. Appl. Phys., vol.41, no.1, pp.64–68, 1970.

[12] C. Elliot and J. Ockendon, Weak and Variational Methods for Moving Boundary Problems, Pitman Publishing, 1981.

[13] R. Sabelka, Dissertation, Technische Universität Wien, 2001.

[14] E. Arzt, O. Kraft, W.D. Nix, and J.E. Sanchez, "Electromigration failure by shape change of voids in bamboo lines," J. Appl. Phys., vol.76, no.3, pp.1563–1571, 1994.

Hajdin Ceric was born in Sarajevo, Bosnia and Hercegovina, in 1970. He studied electrical engieering at the Electrotechnical Faculty of the University of Sarajevo and the 'Technische Universität Wien,' where he received the degree of 'Diplomingenieur' in 2000. He joined the Institut für Mikroelektronik in June 2000, where he is currently working on his doctoral degree. His scientific interests include interconnect and process simulation.

Siegfried Selberherr was born in Klosterneuburg, Austria, in 1955. He received the degree of 'Diplomingenieur' in electrical engineering and the doctoral degree in technical sciences from the 'Technische Universität Wien' in 1978 and 1981, respectively. Dr. Selberherr has been holding the 'venia docendi' on 'Computer-Aided Design' since 1984. Since 1988 he has been the head of the 'Institut für Mikroelektronik' and since 1999 he has been dean of the 'Fakultät für Elektrotechnik.' His current topics are modeling and simulation of problems for microelectronics engineering.